

# Dehydrated and Cs<sup>+</sup>-Exchanged MFI Zeolites: Location and Population of Cs<sup>+</sup> from In Situ Diffraction Data as a Function of Temperature and Degree of Exchange

**Bernard F. Mentzen\***

5 Rue Marcel Desplaces, F-69330 Meyzieu, France

**G rard Bergeret**

IRC (Institut de Recherches sur la Catalyse), CNRS, 2 Avenue Albert-Einstein, F-69626 Villeurbanne, France

**Hermann Emerich**

SNBL (Swiss-Norwegian Beam Lines), ESRF (European Synchrotron Radiation Facility), 6 Rue Jules-Horowitz, P.O. Box 220, F-38043 Grenoble, France

**Hans-Peter Weber**

ACCE, F-38960 St Aupe, France, and LCr/IPMC/ BSP, Swiss Federal Institute of Technology, CH-1015 Lausanne, Switzerland

Received: September 15, 2005; In Final Form: October 20, 2005

H-MFI type zeolitic materials of different Si/Al ratios have been completely or partially cesium-exchanged (cesium content ranging from 0.7 to 7.7 Cs/unit-cell (uc)). Examined with synchrotron X-ray powder diffractometry, an anhydrous sample with the Cs<sub>6.6</sub>H<sub>0.3</sub>Al<sub>6.9</sub>Si<sub>89.1</sub>O<sub>192</sub> chemical composition revealed at ambient temperature the presence of five discrete Cs locations: Cs1 located in the channel intersection near a 10-ring window of the zigzag channel; Cs2 and Cs2', both located in the straight channel but 1.23   apart; Cs3 and Cs3', both located in the zigzag channel and rather close to each other (2.51  ). The populations of the Cs species amounted to 2.61/0.81/1.85/0.86/0.47/uc for Cs1/2/2'/3/3', respectively. The continuous but multimodal nature of the C2 split site is well-described by a joint-probability density function. The 10-ring of the straight channel in the framework is highly elliptical ( $\epsilon = 1.218$ ). The populations for the same sites were also determined at higher temperatures: 131, 237, 344, and 450  C. At 450  C, Cs2' has migrated toward the center of the channel intersection, and the site separation between Cs2 and Cs2' has lengthened to 2.23  . Using a temperature-controlled laboratory X-ray diffractometer, similar studies were carried out on partially or almost totally Cs-exchanged samples from various sources with differing Cs contents. They show that over the 0.7 to 4 Cs/uc range all the individual Cs populations vary linearly as a function of total Cs/uc present. At higher total Cs/uc content (4 to ~7 Cs/uc) solely Cs1 continues to do so. For Cs2+Cs2' and Cs3+Cs3', the variation is almost linear over the whole concentration range. Computer simulations using a 6-exp-1 Buckingham-type atom–atom van der Waals interaction model yield six possible Cs sites in the actual Cs<sub>6.6</sub>MFI framework structure. Four of them lie very close to those determined from difference Fourier maps using the room temperature data. A fifth one is close to the Cs2' species after thermal migration at 450  C, and the sixth one is close to the center of the channel intersection. However, this latter site is observed experimentally only in the case of hydrated CsMFI phases. In the anhydrous Cs<sub>6.6</sub>MFI phase at room temperature, the shortest Cs-framework oxygen distance is Cs3'–O25 = 3.08  , and the next shortest distances are Cs1–O26 = 3.37, Cs2–O11 = 3.34, Cs2'–O22 = 3.47, and Cs3–O20 = 3.34  . The framework T(Si, Al) sites most involved in these contacts are the T9, T11, T12, T10, and T3 sites. This implies that these sites are prime candidates for Si/Al substitution.

## 1. Introduction

Among mineral catalysts of industrial importance, zeolites are particularly attractive materials to investigate: their synthesis is easily reproducible, and the structure of the catalytically active surface can be well-determined at the atomic level. This is rarely the case for their noncrystalline silica–alumina counterparts. For zeolites with promising catalytic properties, a lot of effort has been spent on optimizing these and gaining an understanding of the reactions involved at the microscopic level. The three main prerequisites for high-yield catalysis are (a) an abundance

of Br nsted acid sites, (b) the existence of electrical fields strong enough to polarize the C–C or O–H bonds of molecules residing in the zeolite cavities, and (c) cavities on the scale of these molecules and shaped such that they can properly orient themselves for the reaction. Isomorphous substitution of silicon for aluminum in the framework is the main mechanism involved in the creation of acid sites as the negative charges generated in the structure need to be compensated by protons or counter-cations.

The present study derives its significance, in part from the localization of these acidic sites in MFI(Mobil-five)-type zeolites,<sup>1</sup> by determining the positions of Cs counter-cations.

\* Corresponding author e-mail: mentzen.b@infonie.fr.

More generally though, the present work aims at providing accurate benchmark structures for theoretical modeling. The complexity of the catalytic processes is such that it is far too optimistic to expect their full characterization solely from experimental observations. Computer simulation is needed to fill in the observational gaps, but it should not substitute itself for a feasible experiment. Furthermore, such modeling must be based on sound and complete structural data, or it will yield misleading insights. Finally, another aspect of this work is its immediate relevance to nuclear waste disposal: the Cs<sup>137</sup> isotope is among the most radioactive elements in nuclear waste from reactor operations, and ion exchangers, including zeolites, are being used to remove cesium from solutions stored in long-term tanks.

MFI-type microporous materials belong to the pentasil zeolites. Their framework is built up from 5–1 secondary building units (SBU). The pore system of the MFI framework structure consists of medium-sized cavities, also known as channel intersections (sites **I**), which are interconnected through straight channel sections (sites **III**) by 10-ring pore openings in the [010] axis direction and zigzag (also called sinusoidal) channel sections (sites **II**) by 10-ring pore openings in the [100] axis direction. Depending on the amount, the nature, and the location of extra framework species (essentially adsorbed molecules and/or exchanged cations) in the MFI pores, the 10-ring pore openings range from almost circular ( $8.25 \times 7.99 \text{ \AA}$  in the silicalite-4tetrapropylammonium (TPA) zigzag channels)<sup>2</sup> to highly elliptical ( $9.23 \times 7.07 \text{ \AA}$  in the silicalite-8paranitroaniline straight channels).<sup>3</sup> Labeling of the adsorption sites and some structure correlations between the MFI silicalite framework symmetry and the location or the geometry of adsorbed molecules are reported in ref 4.

Depending on the Si/Al ratio, zeolitic microporous materials with the MFI structural framework type are known either as ZSM-5 (for Si/Al usually less than 100) or as silicalite (Si/Al greater than 150 and highly dealuminated solids).<sup>1</sup> The MFI framework is very flexible, and at least four guest-induced framework polymorphs are known at room temperature: a monoclinic  $P2_1/n11$  (**M**) for the empty silicalite<sup>5</sup> and all the silicalite/*n*-alkanes complexes;<sup>6</sup> a first orthorhombic one with the  $Pnma$  space group (SG) (**O1**);<sup>2</sup> a second orthorhombic one with the SG  $P2_12_12_1$  (**O2**) for the silicalite-8para-xylene complex;<sup>7</sup> and a third orthorhombic one with the SG  $Pn2_1a$  (**O3**) for the optically active (SHG) silicalite-4paranitroaniline complex (presently the sole example for this symmetry).<sup>3</sup>

Compared to cation locations in FAU-type zeolites (faujasites Y and X),<sup>1,8</sup> very little structural information on cationic locations has been reported so far in the literature on cation-exchanged MFI phases. Attempts have been made in MFI containing Ni,<sup>9</sup> Cs,<sup>10</sup> and Tl<sup>11</sup> and for Na, Ni, Cs, and Pb.<sup>12</sup> In a Cs<sub>3.8</sub>-ZSM-5-2.6*p*-xylene complex, three Cs sites have been characterized.<sup>13</sup> One of these cations (Cs2) is  $\pi$ -bonded to the hexagonal carbon ring of the adsorbed *p*-xylene molecule. More recently the same cation has been located at three (at least) locations in a dehydrated Cs<sub>5.8</sub>-ZSM-5 phase:<sup>14</sup> Cs1 and Cs3 are very close to the corresponding sites reported in ref 13, whereas C2 in ref 14 is located in the straight channel and has possibly migrated toward the *p*-xylene aromatic ring.

Cation migration, often evoked in computer simulations but seldom evidenced by structural investigations, is an additional effect that urgently needs to be experimentally characterized before one engages in any simulation. Cation migration might be due to several factors such as the temperature, the sorbate loading (adsorption or desorption), or both. It has been shown

**TABLE 1: Composition from Chemical Analysis, Cs Exchange %, Source and Full-Width at Half-Maximum (fwhm) at 15° (2 $\theta$ -Cu K $\alpha$ ) of the Cs-Exchanged MFI Materials**

Al/uc <sup>a</sup>	Si/Al	Cs/uc <sup>a</sup>	H/uc <sup>a</sup>	Cs exchange (%)	source	fwhm (°)	uc/V (Å <sup>3</sup> )
1.4	70	0.7	0.7	50	Conteka	0.129	5341
3.4	27	2.3	1.1	68	Degussa	0.190	5340
3.6	26	2.0	1.6	56	TPA	0.143	5326
3.8	24	1.6	2.2	42	TPAF	0.116	5344
4.4	21	3.5	1.1	80	TPAF	0.104	5333
4.6	20	2.1	2.5	46	TMP-less	0.107	5361
5.8	15.6	5.3	0.5	91	ref 14	[14]	5338
6.9	14	6.6	0.3	96	TMP-less	0.126	5336
8.2	10.7	2.9	5.3	35	TPAF	0.111	5347
8.2	10.7	3.2	5.0	39	TPAF	0.115	5349
8.8	10	4.0	4.8	45	TPA	0.172	5336
8.8	10	5.4	3.4	61	TPA	0.178	5323
8.8	10	7.7	1.1	88	TPA	0.188	5315

<sup>a</sup> The Al, Cs, and H/uc values are rounded off to the nearest tenth.

experimentally<sup>15,16</sup> that cation migration is clearly at cause in the case where the sorbed molecules are polar. If nonpolar molecules are adsorbed, this cationic migration effect is almost negligible. In FAU type structures the usual I, I', II, and III' and less frequently observed III and II' cationic locations are now well-documented. Except for III', they correspond to high-symmetry special positions (16c, 32e, 48f; orders of  $Fd3/Fd3m = 96/192$  in X and Y faujasites respectively), and their populations can be rather important, especially in the case of dehydrated and exchanged X-type faujasites (Si/Al < 1.2).

The present work is a continuation of our preliminary studies on the subject.<sup>12,13</sup> We aim at describing the distribution of Cs cation and water molecules as a function of temperatures in a series of partially (simultaneous presence of cations and protons) or almost totally Cs-exchanged H-MFI materials, ranging from 0.7 to 7.7 Cs/uc. In the following sections only the results concerning the dehydrated phases are reported. Results concerning the hydrated CsMFI phases (for both dehydration and the hydration processes) will be published separately.

## 2. Experimental Section

**2.1. Materials Synthesis.** The starting materials, with the aluminum (Al/uc), Si/Al ratio, cesium (Cs/uc), and proton (H/uc) contents (from chemical analysis) are reported in Table 1. Zeolites from Degussa and Conteka are industrial samples obtained by the usual ZSM-5 synthesis in alkaline medium.<sup>17</sup> TPA stands for laboratory synthesized samples (IRC) using the classical method derived from ref 18. TPAF samples are synthesized in fluoride medium using the tetrapropylammonium fluoride structure directing agent,<sup>19</sup> and TMP-less samples are obtained in a templateless alkaline medium.<sup>20</sup> All the parent ZSM-5 phases were calcined and ammonium-exchanged in aqueous 0.1M NH<sub>4</sub>Cl solutions. After calcination, the resulting H-forms were partially (one exchange) or almost totally (several exchanges) Cs-exchanged (cold and refluxed (70 °C) aqueous 0.1M CsCl solutions) in order to obtain a series of CsMFI phases ranging from 0.7 to 7.7 Cs/uc concentrations (Table 1).

**2.2. Structural Characterization.** X-ray powder diffraction data were collected (1) at the SNBL (Swiss-Norwegian Beam-Lines, Grenoble, France, BM01B synchrotron beam line,  $\lambda = 0.69918 \text{ \AA}$ ; see Table 4 for further experimental details) using locally built temperature- and atmosphere-controlling equipment (samples in quartz capillaries of 0.8 mm i.d.) and (2) at the IRC (Institut de Recherche sur la Catalyse, Villeurbanne, France,

**TABLE 2: Cs Cation Migration and Ellipticities<sup>a</sup> ( $\epsilon$ ) of the Straight Channel 10-Ring Sections vs Increasing Temperatures in Anhydrous Cs<sub>6.6</sub>MFI<sup>b</sup>**

<i>T</i> (°C)	total Cs	Cs1	Cs2	Cs2'	Cs2+Cs2'	Cs3	Cs3'	Cs3+Cs3'	$\epsilon$	Cs2–Cs2'
28	6.6	2.61	0.81	1.85	2.66	0.86	0.47	1.33	1.218	1.23(6)
131	6.6	2.36	0.99	1.77	2.76	0.93	0.53	1.46	1.168	1.50(6)
237	6.6	2.19	1.56	1.21	2.77	1.07	0.58	1.65	1.120	1.56(6)
344	6.6	2.12	1.88	0.96	2.84	1.00	0.65	1.65	1.087	1.94(6)
450	6.6	1.98	2.09	0.87	2.96	0.95	0.72	1.67	1.065	2.23(6)

<sup>a</sup> Ratio between the maximum and minimum O···O distances in the straight channel 10-ring pore openings. <sup>b</sup> The Cs populations are in Cs/uc, and the Cs2–Cs2' site separations are given in Å.

Panalytical X'Pert Pro MPD diffractometer, Cu K $\alpha$  radiation, X'Celerator Panalytical detector) the samples being mounted on the temperature-regulated stainless steel sample-holder (flat reflection geometry) in a controlled atmosphere (dry dinitrogen flow) Anton Paar XRK 900 reactor chamber. In the case of (2), three XRPD profiles were recorded for each sample: the first one corresponds to the room temperature (26 °C) water-saturated phase, the second one corresponds to the anhydrous sample dehydrated at 450 °C, and the third one corresponds to the anhydrous sample at room temperature. The recorded profiles were corrected for instrumental parameters.<sup>21</sup> All the structure refinements were performed by using the Rietveld method (with a locally modified version of the DBW3.2 code<sup>22</sup> and the EXPGUI version of GSAS).<sup>23</sup> In the refinements the smearing-out of certain atomic positions have been approximated with split-atom positions. For the synchrotron-radiation data set at ambient temperature, these are also described in probability space. The program PDF used is part of the program package POP.<sup>24</sup>

### 3. Computational Methodology

To determine potential sites for Cs, molecular mechanics calculations (MM) were carried out using a Simplex-type variable-step algorithm. The charge distributions on the zeolite T(Si) and O framework atoms and the potential energy parameters of the Si<sub>2</sub>O atoms used in this work for the exp-6-1 van der Waals-type Buckingham atom–atom interaction model (eq 1) are detailed in refs 25–28. The total potential energy reads as follows:

$$E_{\text{tot}} = \sum_{j>k} \{ b_j b_k \exp[-(c_j + c_k)r_{jk}] - a_j a_k r_{jk}^{-6} + q_j q_k r_{jk}^{-1} \} \quad (1)$$

*a*, *b*, *c*, and *q* parameters correspond to the long-range attractive, the short-range repulsive, the van der Waals radius, and the very long-range Coulombic terms, respectively. As in the case of extra framework sodium cations,<sup>27,28</sup> similar potential parameters for the cesium cation were adjusted to *a/b/c* = 66.0/680.0/2.21, respectively, in order to obtain about 3.2 Å for an isolated Cs–O contact. The starting Cs cation locations for each of the 26 framework oxygen atoms in the actual (refined) Cs<sub>6.6</sub>MFI structure were positioned such as to yield a O–Cs = 3.2 Å distance, the O–Cs line bisecting the Si–O–Si angle. In each of the 26 cases, the four atoms corresponding to a Cs site and the associated Si–O–Si bridge adopt the planar geometry described in ref 29 or in ref 30 where, instead of Cs cations, preferred proton locations were modeled for orthorhombic and monoclinic H-MFI/benzene systems.

### 4. Results and Discussion

**4.1. Room Temperature (RT: 28 °C) Cs<sub>6.6</sub>MFI Phase.** The starting MFI framework parameters of the Cs<sub>6.6</sub>MFI phase are those reported in ref 13 for an MFI phase with the *Pnma* (O1)

space group symmetry. To obtain the actual framework structure of the zeolite, the low-angle diffraction range (1.524–10° 2 $\theta$ ) was omitted in the first refinement cycles. As pointed out in ref 31, the upper angular range (2 $\theta$  = 10–34.788°) is almost unaffected by the extra framework species. The Rietveld refinement was also performed under geometric restraints (Si–O/O–O = 1.589/2.5948 Å). In the ensuing refinement cycles, the full angular range was included, and the difference Fourier (DF) maps clearly revealed the presence of three major residues corresponding to possible Cs cation sites: Cs1, located in the channel intersection close to a 10-ring opening of the zigzag channel; Cs2, located in the straight channel; and Cs3, located in the zigzag channel at about 3.50 Å of Cs1. These three sites were then introduced into the data stream and the whole structure refined again. At this stage, the total cation concentration amounted to 6.2 Cs/uc. Final DF maps revealed a splitting of Cs2 over two rather close (1.2 Å separation) Cs2 and Cs2' sites and the existence of an additional Cs3' site in the zigzag channel at about 2.5 Å from Cs3. Since the DF peaks of Cs1, Cs3, and Cs3' located on the mirror plane of the *Pnma* structure seemed to spread over both sides of *m* (banana-shaped contour lines), their *y* coordinates were relaxed. After the final refinement cycles, the cesium content amounted to 6.6(2) Cs/uc, in fair agreement with the chemical analysis. The Cs/uc populations for this phase are given in Table 2, and the final atomic positions are reported in Table 3. The Cs1, Cs2, and Cs3 sites refined in the present work are close to those reported in ref 14. The Rietveld plots are shown in Figure 1, and some structural details showing the Cs locations in the MFI framework are given in Figure 2a. The experimental details are reported in Table 4, together with some crystallographic parameters.

Split-atom sites are always indicative of disorder, and their use in a refinement model is a rough and approximate description of reality. Their inherent proximity, coupled with the use of displacement parameters to describe the smearing-out of this type of position, frequently succeed in modeling disorder to the extent that DF maps become almost featureless. However, little physical meaning should be attached to the exact atomic positions themselves. A more revealing picture is obtained by analyzing maps of probability densities instead of electron densities. Let it be recalled that the probability density is the Fourier transform in real space of the (thermal and/or disorder) displacement tensor in reciprocal space. Maps of the probability density—even though their resolutions are subject to the same *d*<sub>min</sub>—reveal the distribution of atoms in greater and sharper detail than Fourier maps because (a) they do not suffer from termination effects, (b) the random noise is filtered out, and (c) the finite-sized electron shell has been deconvoluted out. Figure 3 shows the probability density of the C2 split site. The density in this case is a superposition of the probability density contributed by each split-atom, with the individual contribution weighted by the site occupancy (for a similar approach, using the same formalism, see, for example, ref 32). We now see clearly that in this region of the cavity system the Cs cations

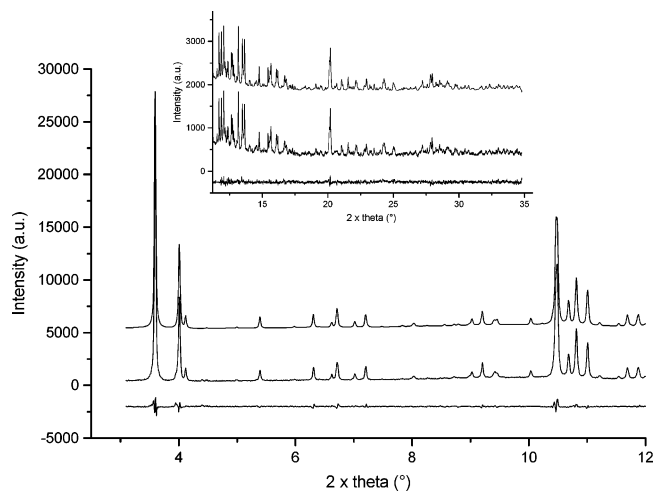
**TABLE 3: Cs<sub>6.6</sub>MFI at Room Temperature (28 °C)**

atom	x	y	z	occ <sup>a</sup>
T1	0.42428(2)	0.05598(2)	-0.34896(3)	
T2	0.30551(2)	0.02934(2)	-0.20358(3)	
T3	0.28048(2)	0.06350(2)	0.01538(3)	
T4	0.12159(2)	0.06447(2)	0.01377(3)	
T5	0.07080(2)	0.03022(2)	-0.19384(3)	
T6	0.18076(2)	0.05624(2)	-0.34114(3)	
T7	0.42183(2)	-0.17170(2)	-0.33545(3)	
T8	0.30485(2)	-0.13014(2)	-0.19402(3)	
T9	0.27655(2)	-0.17351(2)	0.02492(3)	
T10	0.12017(2)	-0.17430(2)	0.02000(3)	
T11	0.06828(2)	-0.12941(2)	-0.19175(3)	
T12	0.18257(2)	-0.17101(2)	-0.32954(3)	
O1	0.36765(3)	0.05351(4)	-0.26640(5)	
O2	0.30605(4)	0.06346(4)	-0.09623(3)	
O3	0.20089(1)	0.05962(4)	0.02095(6)	
O4	0.10148(4)	0.06618(3)	-0.09994(3)	
O5	0.10964(2)	0.05032(4)	-0.29162(4)	
O6	0.23787(3)	0.04824(4)	-0.25930(5)	
O7	0.36689(3)	-0.15882(4)	-0.25286(5)	
O8	0.30572(4)	-0.15829(4)	-0.08269(3)	
O9	0.19819(1)	-0.15820(3)	0.02550(6)	
O10	0.09537(4)	-0.16274(4)	-0.09158(3)	
O11	0.11063(2)	-0.15287(4)	-0.28590(4)	
O12	0.23763(3)	-0.15201(4)	-0.24868(5)	
O13	0.30905(4)	-0.05020(1)	-0.19034(6)	
O14	0.07479(4)	-0.04961(1)	-0.17905(6)	
O15	0.42026(3)	0.12610(3)	-0.40648(5)	
O16	0.41224(4)	-0.00242(3)	-0.42908(5)	
O17	0.40328(4)	-0.13208(3)	-0.43456(4)	
O18	0.18773(4)	0.12767(2)	-0.39355(5)	
O19	0.19015(4)	-0.00047(3)	-0.42429(5)	
O20	0.19579(4)	-0.13048(3)	-0.42921(4)	
O21	-0.00597(2)	0.04903(4)	-0.20431(5)	
O22	-0.00770(2)	-0.14861(4)	-0.20593(5)	
O23	0.42426(6)	-1/4	-0.36102(7)	
O24	0.18571(6)	-1/4	-0.35195(8)	
O25	0.28816(6)	-1/4	0.05314(7)	
O26	0.10806(6)	-1/4	0.05134(7)	
Cs1	0.0547(4)	0.2530(35)	0.8845(6)	0.326(7)
Cs2	-0.0225(28)	0.0586(27)	0.4442(27)	0.101(7)
Cs2'	0.0376(12)	0.0680(11)	0.4313(12)	0.231(7)
Cs3	0.2271(11)	0.2551(57)	0.9288(19)	0.108(2)
Cs3'	0.2796(24)	0.2641(59)	0.7590(30)	0.059(3)

<sup>a</sup> T and O framework sites are fully occupied.  $U_{\text{iso}}$  (Å<sup>2</sup>) of Si/O/Cs = 0.0168(38)/0.024(9)/0.143(40).

are distributed in a continuous fashion, with local maxima at Cs2 and Cs2'. This situation is likely to prevail up to about 200 °C. At 237 °C, the split sites have become genuinely distinct and are more than 1.9 Å apart.

Another unexpected structural detail is the rather high ellipticity of the straight channel 10-ring section ( $\epsilon = 1.218$ ). In ref 14 this ellipticity is notably lower ( $\epsilon = 1.147$ ). Usually, elliptical straight channel or zigzag channel sections appear in case of tight-fitting sorbents<sup>4</sup> [as for instance in silicalite•4*p*-xylene (SC,  $\epsilon = 1.184$ ),<sup>26</sup> silicalite•8*p*-xylene (SC,  $\epsilon = 1.184$  and ZZ,  $\epsilon = 1.217$ ),<sup>7</sup> silicalite•6benzene (ZZ,  $\epsilon = 1.213$ ),<sup>33</sup> silicalite•8benzene (SC,  $\epsilon = 1.223$ ),<sup>33</sup> silicalite•4tetrachlorethylene (SC,  $\epsilon = 1.160$ ),<sup>34</sup> silicalite•8tetrachlorethylene (SC,  $\epsilon = 1.195$  and ZZ,  $\epsilon = 1.195$ ),<sup>34</sup> and silicalite•8*p*-nitroaniline (SC,  $\epsilon = 1.304$  and ZZ,  $\epsilon = 1.246$ ),<sup>3</sup> presently the most elliptical channel deformation observed in an MFI material]. Accordingly, in dehydrated Cs<sub>6.6</sub>MFI, one might conclude that specific cation-framework interactions exist between the Cs2, Cs2' cations and oxygen (or even T) atoms in the straight channel and that these are responsible for the increased ellipticity. We have verified that the 10-ring pore openings in the framework structure of the parent zeolite and its H-form are not significantly elliptical.



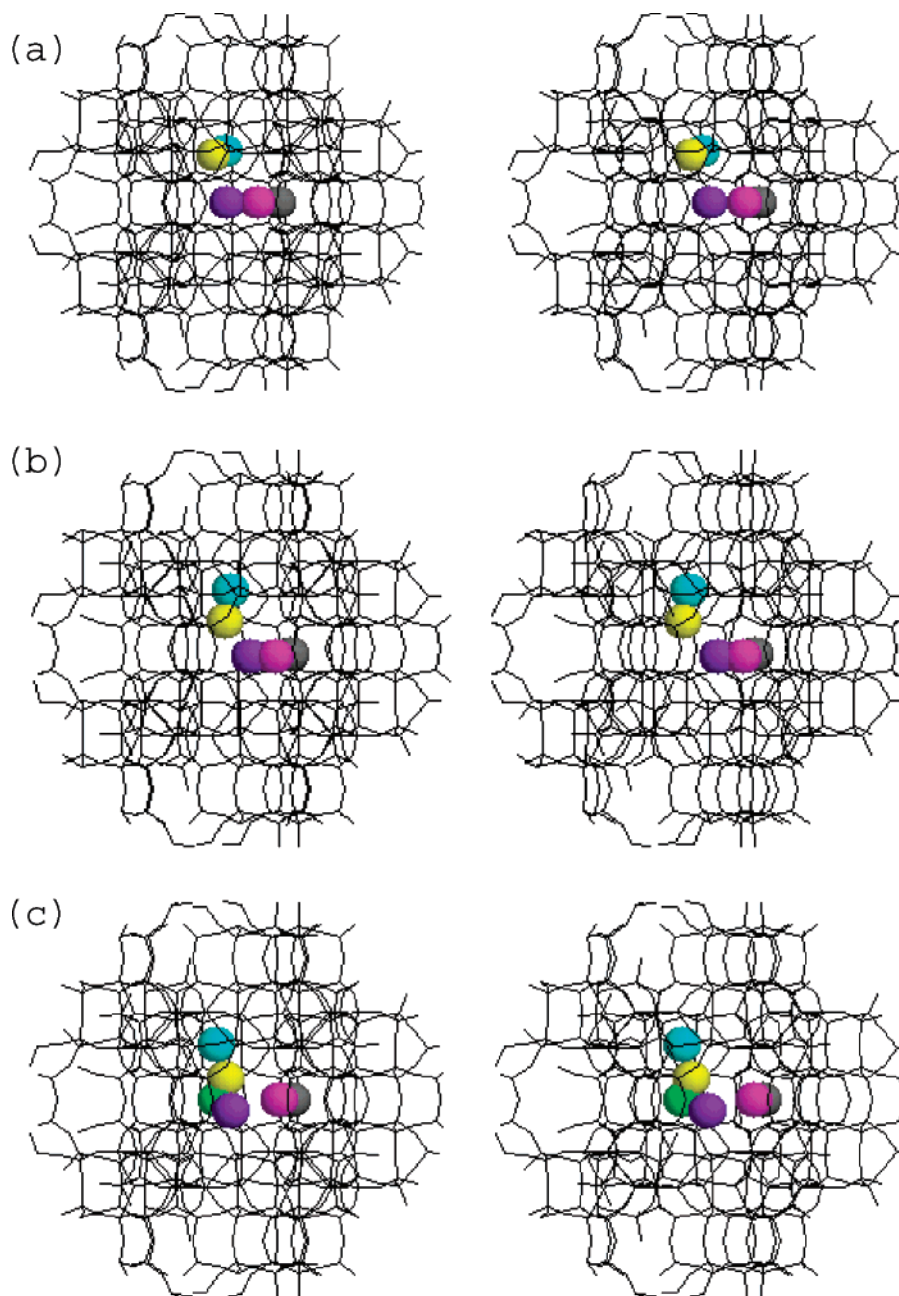
**Figure 1.** Rietveld plots for the dehydrated Cs<sub>6.6</sub>MFI phase at room temperature: calculated (lower trace), observed (middle trace), and difference (lower trace) profiles.

Table 5 lists some short Cs–O and Cs–Si(Al) contacts. In inorganic phases *not* involving water molecules, short Cs–O distances are observed in the 2.84(1)<sup>35</sup> to 3.118(3) Å range.<sup>36</sup> In zeolitic phases, some short Cs–O contacts are also observed (e.g., 2.97(2), 3.1(1) Å and even shorter (2.5(2) Å; Cs in site I, D6R hexagonal prism) in an X faujasite;<sup>37</sup> 2.95(7) Å in a Y faujasite;<sup>16</sup> and 3.19, 3.24 and 3.29 Å in mordenite.<sup>38</sup>

The question now arises how these Cs distributions correlate with the overall Cs/uc amount in other Cs-exchanged MFI materials. This point is broached in section 4.3. The following section reports on the evolution of the crystal structure of Cs<sub>6.6</sub>-MFI as a function of increasing temperature.

**4.2. Cation Migration: High Temperature (HT) Cs<sub>6.6</sub>MFI Phases.** The four XRPD data collections at 131, 237, 344, and 450 °C have been interpreted in the same manner as the room temperature one. In addition to the usual Si–O/O–O restraints, the sum of the individual Cs populations were constrained to 6.6 Cs/uc. At higher temperatures the refined mean overall  $U_{\text{iso}}$  thermal parameters of the Si/O/Cs atoms are 0.016(1)/0.029(4)/0.15(1), respectively. Given their rather slight variation versus temperature and for the sake of simplicity, they were fixed to those of the RT (28 °C) values. The variations of the five cesium cation populations, of the Cs2–Cs2' site separations and of the elliptical straight channel 10-ring sections versus temperature are given in Table 2. The Cs cation locations in the HT phase are compared to those in the RT one in Figure 2b. The other structural parameters are reported in Tables 1S–4S (Supporting Information). The unit-cell parameters of the Cs<sub>6.6</sub>MFI phases versus temperature are given in Table 6. Selected short Cs–O and Si(Al)–O distances are given for the high-temperature phases in Tables 5S–8S (Supporting Information). As the temperature increases, the ellipticities ( $\epsilon$ ) of the straight channel 10-ring sections decrease almost linearly with T. Shorter Cs–O contacts appear, specially at 450 °C, where the shortest Cs2'–O7(T7,T8) = 2.87(6) and Cs3–O20(T3,T12) = 2.96(6) Å distances are comparable to those in refs 37 and 39 and Table 8S (Supporting Information). The migration of the individual Cs cations, including split-atom sites, versus temperature are represented in Figure 5.

**4.3. Cs Siting and Populations versus Cs/uc Content.** The question now arises: are the structural correlations between Cs locations and populations transferable to Cs-exchanged MFI material of different stoichiometry? To answer this question, the XRPD profiles corresponding to the 12 samples reported in



**Figure 2.** Structural detail showing the cesium cations in the MFI framework. Stereopair projections down the [100 zigzag channel] direction. (a) The structurally refined Cs cations and their labeling and coloring scheme. (b) The same cations after migration at 450 °C. (c) The simulated Cs locations (molecular mechanics). Coloring scheme: gray/yellow/cyan/magenta/purple and green for Cs1/Cs2/Cs2'/Cs3/Cs3' and Cs6, respectively.

Table 1 were analyzed by the Rietveld method. For comparison, some data reported in ref 14 are also mentioned in Table 1. The resulting Cs distributions and the corresponding unit-cell parameters are reported in Tables 7 and 8, respectively. The evolution of the individual Cs1/uc, Cs2/uc+Cs2'/uc, and Cs3/uc+Cs3'/uc populations versus total cesium content are shown in Figure 6. For some of the dehydrated CsMFI samples, the XRPD profiles recorded at high temperature (450 °C) were also analyzed, and the corresponding Cs/uc distributions are reported in Figure 7.

Over the  $0.7 < \text{Cs/uc} \leq 4.0$  concentration range, the Cs1, Cs2+Cs2', and Cs3+Cs3' populations increase almost linearly with concentration (Figure 6). For higher cesium contents ( $>4\text{Cs/uc}$ ) Cs1/uc increases less and Cs3/uc+Cs3'/uc increases more. The changes in slope of these two lines at *exactly* 4Cs/uc correlate directly with possible changes in the MFI framework symmetry. Solid-state polymorphic phase transitions have

been observed in many MFI type sorbent/sorbate complexes for this critical 4 sorbed molecules/uc loading. As Cs cations distributed over three main locations can hardly be considered "adsorbed molecules", the driving force which induces the observed effect should be of a different nature. Apparently, the Cs1/uc slope change occurs at exactly 2Cs1/uc (for a total of 4Cs/uc), and this cation location is the most populated one. Structural changes occurring at 2 molecules/uc are observed in several silicalite/sorbate systems, as for instance in silicalite·2*p*-xylene<sup>40,41</sup> and in silicalite·2tetrachlorethylene.<sup>34</sup> But these effects only appear in the case of poly-phased MFI systems.<sup>42</sup> In the present case, all the refined XRPD profiles correspond to single-phased materials and, except for the first sample containing 0.7Cs/uc (monoclinic  $P2_1/n11$  space group), all the investigated CsMFI solids show straight channel 10-ring openings that are elliptical. As already mentioned, this ellipticity is usually the consequence of specific interactions between ex-

**TABLE 4: Experimental and Selected Crystallographic Parameters for the Cs<sub>6,6</sub>MFI Phase at Room Temperature (28 °C)**

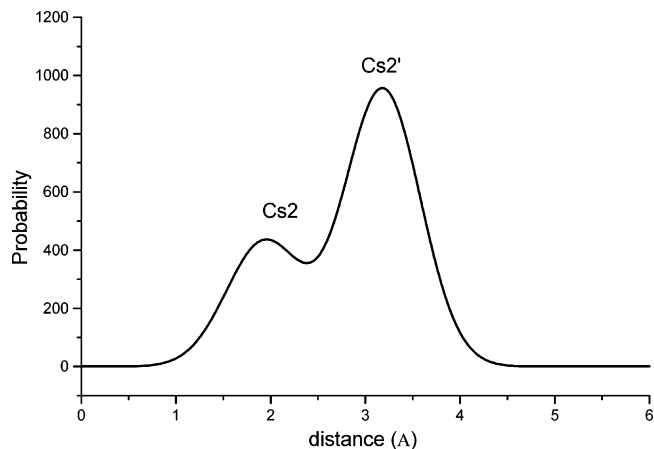
chemical formula	Cs <sub>6,6</sub> H <sub>0,3</sub> Al <sub>6,9</sub> Si <sub>89,1</sub> O <sub>192</sub>
space group	Pnma
powder diffractometer	SNBL BM01B beam-line, custom-built, 6 detectors with Si (111) monochromators
scan range (2θ°)	1.524–34.788
profile function (U, V, W, etc.)	pseudo-Voigt (4 parameters)
wavelength (Å)	0.69918
step size (2θ°)	0.004
counting time (s)	1
no. of background points (linear interpolation)	40
no. of data points	8317
no. of contributing reflections (hkl)	1827
no. of refined structural parameters	138
a (Å)	19.9933(3)
b (Å)	19.9367(2)
c (Å)	13.3873(2)
Rp/Rwp/Rexp/R(F <sup>2</sup> ) (%)	3.62/4.75/4.01/4.58
Si–O/O···O restraints (Å)	1.589/2.5948 (~ideal T <sub>d</sub> )
refined Si–O range (Å)	1.572–1.605 (mean 1.589)
N – P + C	7873
sample temperatures (°C)	28, 131, 237, 344, 450
heating conditions	dynamic vacuum, regulated hot air gun

traframework species and the MFI structure *in* or through the straight channel.<sup>4</sup> Since the Cs1 ions are rather far from the straight channels, one possibility is a conjugate effect of the most populated Cs1+Cs2+Cs2' cations. A second possibility is the occurrence of a  $Pnma \rightarrow P2_12_12_1$  or a  $Pnma \rightarrow Pn2_1a$  phase transition, which cannot be unambiguously detected by XRPD. No slope change is observed for the Cs2/uc+Cs2'/uc line versus total Cs/uc. Apparently at 7.7 Cs/uc the cation populations are not aligned on the three correlation lines represented in Figure 6. This exception might be the result of structure defects or a decrease in the crystallinity for this very highly cesium loaded Cs<sub>7,7</sub>MFI phase.

At high temperature (450 °C) the three lines representing the evolutions of the Cs1, Cs2+Cs2' and Cs3+Cs3' populations versus total Cs/uc (Figure 7) might be considered as almost linear with only a slight slope change for Cs1. It must be emphasized that with increasing temperature the ellipticities of the straight channel 10-ring openings decrease toward almost circular sections (Table 2).

**TABLE 5: Selected Cation to Framework-Anion Bonds and Cation to Framework-Cation Distances in the Cs<sub>6,6</sub>MFI Phase at 28 °C<sup>a</sup>**

atom pair	distance	T sites	atom pair	distance	T sites	atom pair	distance	T sites
Cs1–O26	<b>3.37</b> (1)	T10x2	Cs2–O11	<b>3.33</b> (5)	T11,12	Cs2'–O22	3.47(2)	T4,7
Cs1–O23	3.43(1)	T7x2	Cs2–O5	3.45(5)	T5,6	Cs2'–O13	3.49(2)	T2,8
Cs1–O17	3.44(5)	T4,7	Cs2–O19	3.55(6)		Cs2'–O7	3.61(2)	
Cs1–O15	3.62(5)		<b>Cs2–Si11</b>	3.77(4)		<b>Cs2'–Si8</b>	3.78(2)	
<b>Cs1–Si10</b>	3.99(3)		<b>Cs2–Si5</b>	3.91(4)				
			<b>Cs2–Si3</b>	3.98(5)				
Cs3–O20	<b>3.34</b> (8)	T12,3	Cs3'–O25	<b>3.08</b> (4)	T9x2			
Cs3–O24	3.41(3)	T12x2	Cs3'–O18	3.49(8)	T6,9			
Cs3–O20	3.48(8)	T3,12	Cs3'–O9	3.51(6)				
<b>Cs3–Si12</b>	3.98(5)		Cs3'–O26	3.58(5)				
<b>Cs3–Si3</b>	3.9(1)		<b>Cs3'–Si9</b>	3.78(7)				
			<b>Cs3'–Si9</b>	3.55(6)				
			<b>Cs3'–Si10</b>	3.96(5)				

<sup>a</sup> Only distances less than 3.6 for Cs–O and 4.0 Å for Cs–Si(Al) are given.**Figure 3.** Relative probability density (scaled-up to 1000 for the highest value) of the Cs(2) split position.**TABLE 6: Unit-Cell Parameters (Å) and Volume (Å<sup>3</sup>) of Cs<sub>6,6</sub>MFI Phases vs Temperature**

a	b	c	V	T (°C)
19.9933(3)	19.9367(2)	13.3873(2)	5336.2(1)	28
20.0308(3)	19.9465(3)	13.3988(2)	5353.4(1)	131
20.0656(2)	19.9462(2)	13.4073(2)	5366.0(1)	237
20.0845(2)	19.9412(2)	13.4083(2)	5370.1(1)	344
20.0861(2)	19.9381(2)	13.4069(2)	5369.2(1)	450

These results show that in all the CsMFI phases investigated so far the individual Cs cation populations correlate well with the total Cs amount. Accordingly, the mechanism of Cs incorporation in H-MFI materials is independent from the source of the material (industry, laboratory) or the Cs-exchange percentage (partial or total, presence of unexchanged protons).

**4.4. Computer Simulation of Cs Location.** Our previous computer simulations [25–28] have shown that locations and orientations of sorbed molecules in MFI type materials could only be predicted reliably when the actual framework structures were known. In other words, a precise knowledge of the crystal structure is a prerequisite to any attempt to model zeolitic sorbent/sorbate systems, and even then the use of this knowledge is no guarantee for the success of a simulation (see, for example, ref 14). This is also true when using simulation techniques to locate extraframework cations.

As detailed in section 3, 26 Cs starting locations (one for each oxygen atom in the *Pnma* MFI structure) were calculated using the Cs<sub>6,6</sub>MFI framework as refined. After energy-minimization, only six possible sites remained. These sites are reported in Table 9 and compared in Figure 2c with the

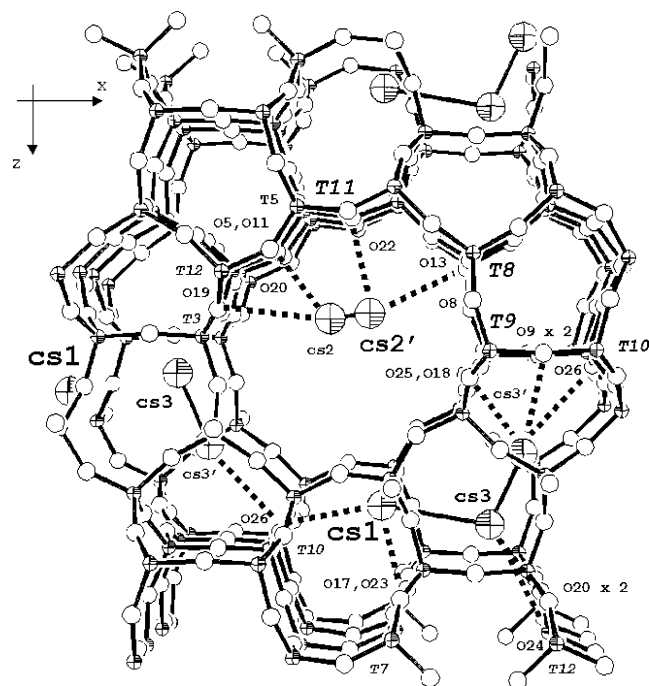


**Figure 4.** Five Cs cations in the Cs<sub>6,6</sub>MFI framework at room temperature and their closest Cs–O and Cs–Si(Al) contacts.

**TABLE 7: Populations of the Cs Cations (Cs/uc) and Straight Channel Ellipticities ( $\epsilon$ ) in CsMFI Materials at 28 °C**

total Cs <sup>a</sup>	Cs1	Cs2	Cs2'	Cs2+Cs2'	Cs3+Cs3'	$\epsilon^b$	uc/V (Å <sup>3</sup> )
0.7	0.50	0.00	0.00	0.00	0.20	1.071	5341
1.6	0.95	0.11	0.32	0.43	0.21	1.144	5344
2.0	1.09	0.25	0.34	0.59	0.30	1.141	5326
2.1	1.19	0.20	0.40	0.60	0.28	1.138	5361
2.3	1.18	0.00	0.69	0.69	0.44	1.149	5340
2.9	1.38	0.41	0.62	1.02	0.40	1.177	5347
3.2	1.61	0.50	0.66	1.16	0.46	1.185	5349
3.5	1.79	0.27	0.98	1.25	0.47	1.186	5333
4.0	1.97	0.60	0.90	1.50	0.53	1.181	5336
5.3 <sup>c</sup>	2.35	2.09		2.09	0.88	1.147	5338
5.4	2.21	1.20	1.04	2.24	0.95	1.204	5323
6.6	2.61	0.81	1.85	2.66	1.33	1.218	5336
7.7	2.00	1.37	2.39	3.76	1.94	1.199	5314

<sup>a</sup> From chemical analysis. <sup>b</sup> Ratio between the maximum and minimum O···O distances in the straight channel 10-ring pore openings. <sup>c</sup> Ref 14.

previously refined Cs locations (Figure 2a,b). It is gratifying how close predicted and refined Cs locations lie. This contrasts with ref 14 where the 12 predicted and refined Cs sites lie rather

**TABLE 8: Unit-Cell Parameters (in Å) for the Investigated Cs-Exchanged MFI Materials at 28 °C**

total Cs	<i>a</i>	<i>b</i>	<i>c</i>	$\alpha$ (°)	$\epsilon$	uc/V (Å <sup>3</sup> )	R(F <sup>2</sup> ) %
0.7	20.0666(6)	19.8926(8)	13.3806(6)	90.201(3) <sup>a</sup>	1.071	5341.2(4)	6.2
1.6	20.0578(5)	19.9055(5)	13.3859(4)		1.144	5344.4(4)	4.5
2.0	20.0253(7)	19.8908(8)	13.3704(6)		1.141	5325.7(7)	4.9
2.1	20.0782(5)	19.9291(5)	13.3991(5)		1.138	5361.5(5)	5.5
2.3	20.0574(7)	19.9042(7)	13.3766(6)		1.149	5340.3(6)	4.0
2.9	20.0447(7)	19.9195(7)	13.3919(5)		1.177	5347.1(6)	7.4
3.2	20.0466(5)	19.9213(5)	13.3954(4)		1.185	5349.5(4)	4.8
3.5	20.0259(5)	19.9050(5)	13.3798(4)		1.186	5333.4(4)	5.5
4.0	20.042(1)	19.902(1)	13.3774(9)		1.181	5336(1)	6.8
5.3	20.0045(5)	19.9229(4)	13.3929(4)		1.147	5337.7(3)	5.3
5.4	20.0172(9)	19.8963(9)	13.3664(8)		1.204	5323(1)	5.5
6.6	19.9933(3)	19.9367(2)	13.3873(2)		1.218	5336.2(1)	4.6
7.7	19.989(1)	19.897(1)	13.362(1)		1.199	5314(1)	8.6

<sup>a</sup> This phase is monoclinic with *P*2<sub>1</sub>/*n*11 framework symmetry ( $\alpha$  deformation angle as reported in ref 5).

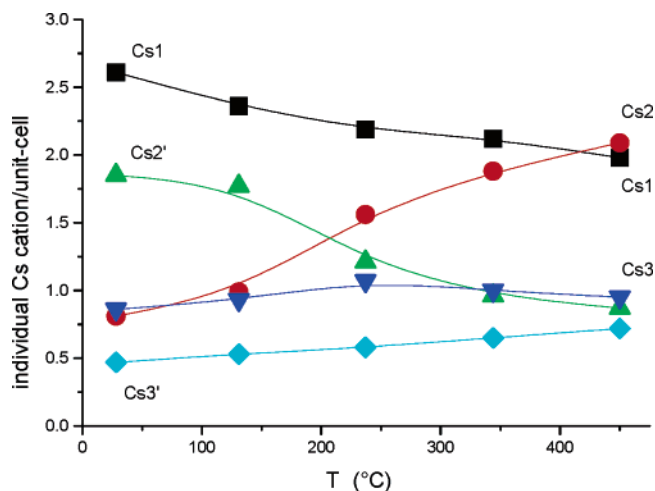


**Figure 5.** Migration vs temperature of the five Cs cations in Cs<sub>6,6</sub>-MFI. At each temperature, the sum of the individual cations is fixed at 6.6Cs/uc.

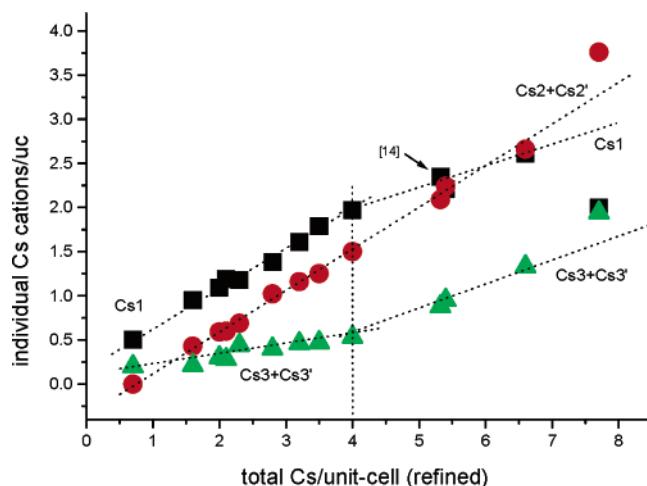


**Figure 6.** Evolution of the individual Cs1/uc (squares), Cs2/uc+Cs2'/uc (circles), and Cs3/uc+Cs3'/uc (triangles) populations vs total Cs/uc content at room temperature.

far apart. Still, we were not able to simulate the Cs2–Cs2' site splitting for the room temperature case because these two sites are too close, but we could simulate it for the high-temperature MFI framework. The sixth site predicted cannot be attributed to a Cs cation in any of the investigated CsMFI phases. In a forthcoming paper, we will show that this site corresponds to one of the six independent water molecules (ow3) found in the completely hydrated Cs<sub>6,6</sub>MFI phase. This apparent confusion

**TABLE 9: Comparison of the Simulated (MM) and Refined (Rietveld) Cs Locations in Cs<sub>6,6</sub>MFI**

simulated locations (MM)			refined locations (Rietveld)			site
x	y	z	x	y	z	
0.04696	0.24888	0.89780	0.0547(4)	0.2530(35)	0.8845(6)	Cs1
0.04062	0.05150	0.39241	-0.0225(28)	0.0589(27)	0.4442(27)	Cs2
			0.0376(12)	0.0680(11)	0.4313(12)	Cs2'RT
0.03223	0.17282	0.44453	0.0378(15)	0.1475(19)	0.4353(23)	Cs2' HT
0.20059	0.25072	0.97225	0.2271(11)	0.2251(57)	0.9288(19)	Cs3
0.29957	0.29211	0.75937	0.2796(24)	0.2641(59)	0.7589(30)	Cs3'
0.04739	0.24991	0.40353	0.0361(16)	1/4	0.4265(25)	ow3 <sup>a</sup>

<sup>a</sup> ow3 is a water molecule observed in the hydrated Cs<sub>6,6</sub>MFI·28H<sub>2</sub>O phase (forthcoming report).

**TABLE 10: Si/Al Substitution in the MFI Framework: A Comparison between Results Deduced from Experimental and Theoretical Work<sup>a</sup>**

probable <sup>b</sup>	less probable	ref/year	method
Si/Al Substitution in MFI (ZSM-5)			
T9,11,12,10,3	T4,5,6,7	this work	closest Cs—O distances
T4,7,10,11,12	T2,8,9	14/2000	closest Cs—O distances
T1,2,8,9,11,12	T3,5,6	33/1994	H-MFI/benzene complexes and differential adsorption calorimetry
<b>T12</b>		57/1995	simulation
<b>T9</b>	T1,5,12	48/1993	simulation
no preferred sites		46/1992	simulation
T2,9,5,12,6		50/1992	simulation
T6,12,9	T3	58/1991	simulation
<b>T12</b>		59/1991	simulation
T2,8		49/1988	simulation
T2,T12		47/1985	simulation
Si/Ti Substitution in TS-1			
T10,11	T1,2,5,9	51/2000	XRD
homogeneously distributed		52/1999	XRD
randomly distributed		53/1997	simulation
<b>T8</b>		55/1995	simulation
T5,9,3,4	T12,10,7,1,11	56/1994	simulation
T6, T19 (monoclinic)		54/1993	simulation

<sup>a</sup> Values for titanosilicalite (TS-1) are also given for comparison. <sup>b</sup> With most probable in bold.

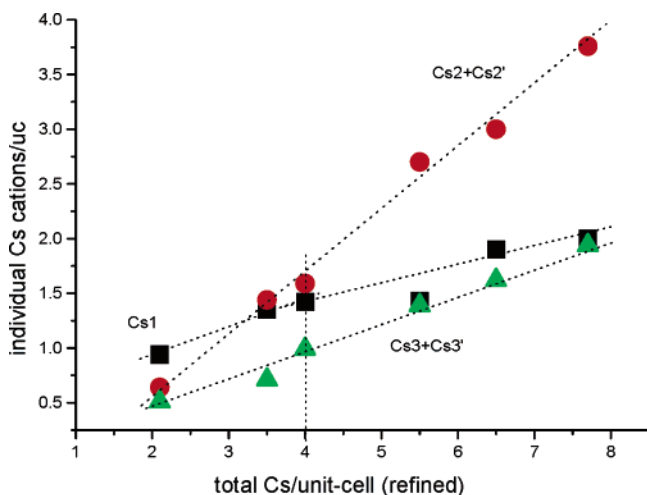


**Figure 7.** Evolution of the individual Cs1/uc (squares), Cs2/uc+Cs2'/uc (circles), and Cs3/uc+Cs3'/uc (triangles) populations vs total Cs/uc content at 450 °C.

between predicted Cs or water locations is not surprising since Cs—O/framework and Cs—O(water) distances are very similar (2.87 to 3.19 Å).<sup>36,43</sup>

**4.5. The Si/Al Substitution Problem.** This work was not intended to be primarily concerned with the Si/Al substitution problem. However, the availability of precise counteranion locations permits us to go now a step further and to use these to bring out the locations of the acidic sites, those where Al substitutes for Si. The theoretical underpinning of this approach comes from ab initio calculations<sup>43,44</sup> and empirical crystal-

chemical rules. The former predict that monovalent cations such as Na<sup>+</sup> or Cu<sup>+</sup> will preferentially attach themselves to oxygen atoms bonded to aluminum, to minimize their interaction energy. The latter predict the same, but based on a balancing of the electrostatic bond strengths reaching an anion from its surrounding cations. This is the second of Pauling's five rules meant to rationalize the stability of inorganic structures. Table 5 lists short Cs—O distances. From this compilation, it is evident that the T(Si,Al) sites involved are mainly T9, T11, T12, T10, and T3. If instead we consider short Cs...Si contacts, then T9, T11, and T8 are favored. The corresponding sites in the structure are shown in Figure 4. Table 10 summarizes the sites found in this and former studies. We have included values for the Ti<sup>4+</sup> substitution in silicalite, even though the situation is not strictly equivalent. In fact, in silicalite there is no need for charge balancing counteranions. However, if we compare the data in Table 10, it seems that there might be some similarity between these two substitution problems: T10, T11, T9, T8, T3, and T4 are invoked in both cases. These data also show that all 12 T1 to T12 sites in an orthorhombic *Pnma* MFI framework structure might be invoked as Si/Al substitution candidates. Nevertheless, in our opinion, only a restricted set of T sites, for instance T2, T3, T9, T12, and possibly T11, might be considered as *plausible* candidates. Furthermore, the framework oxygen atoms bonded to the T2 and T3 sites reside close to the most accessible locations for extra framework species at the border of the channel intersection and the zigzag channel (T2...T2 ~8.8 and T3...T3 ~7.6 Å), whereas the oxygen atoms bonded to T12 and T9 are in a geometrically restricted part of the intersection (T12...T12 ~3.1 and T9...T9 ~3.2 Å), which is in favor of sites T2 and T3.

Whatever the solution, the Si/Al substitution problem is not evident and remains still open for future debates. Based on the results of this and former<sup>14,30</sup> studies, it can be ascertained that Al does substitute for Si and that particular sites are favored. A random substitution can definitely be ruled out.

## 5. Conclusions

The present work is the first instance where the cesium cations in dehydrated and Cs-exchanged MFI materials have been unambiguously located over a wide range of Cs exchange. This permits us to draw the following conclusions:

(1) The Cs cations are distributed over three highly and two less populated sites. The correlations describing the evolution of the Cs populations at room temperature as a function of total Cs/uc contents clearly establish that the mechanism of Cs incorporation into the MFI framework channels is unique.

(2) While it cannot be denied that plausible locations for extraframework cations can be obtained from simulations, these simulations have to be based on observed MFI framework structures because the flexibility of the framework is not yet a predictable parameter in computer modeling. This is why many wrong locations for aromatic molecules in silicalite and ZSM-5 phases have been and are still being predicted, as for instance the benzene locations in silicalite at lower (<4 molecules/uc) and specially at higher (>6 molecules/uc) loadings.

(3) In all *Pnma* CsMFI phases the straight channel 10-ring sections are strongly elliptical ( $\epsilon > 1.14$ , except for the monoclinic sample at 0.7 Cs/uc). This structural feature points to strong Cs/framework interactions.

(4) The short Cs—O distances give us some clues on the possible substitution of Si by Al. The most favored sites are T9, T11, T12, T10, and T3.

Subsequent work on Cs-exchanged MFI will deal with hydrated phases. The following key questions will be answered:

(i) How are the Cs locations affected by the presence of water molecules?

(ii) Where are the water molecules located in such systems? Are there any differences in the dehydration or the hydration process at room or at increasing temperatures?

(iii) Is it possible to simulate the locations of the water molecules?

**Acknowledgment.** We thank J. Patarin, H. Kessler, and A. C. Fauth, Mulhouse (France); A. Tuel, IRC, Villeurbanne (France); and A. Tissler, Mainz (Germany) for the MFI samples prepared in fluoride medium (TPAF), in alkaline medium (TPA), and in templateless alkaline medium (TMP-less), respectively, and the staff of the Swiss-Norwegian Beam Lines for assistance. H.P.W. thanks the Swiss National Science Foundation for steadfast support and the Tisserand Foundation, Montricher, for a fellowship.

**Supporting Information Available:** Refined atomic coordinates and site occupancies for diffraction data collected at 131, 237, 344, and 450 °C; tables of selected interatomic distances for the same temperatures. This material is available free of charge via the Internet at <http://pubs.acs.org>.

## References and Notes

- (1) Baerlocher, Ch.; Meier, W. M.; Olson, D. H. *Atlas of Zeolite Framework Types*, 5th ed.; Elsevier: Amsterdam, 2001.
- (2) van Koningsveld, H.; van Bekkum, H.; Jansen, J. C. *Acta Crystallogr.* **1987**, *B43*, 127–132.
- (3) Mentzen, B. F.; Lefèbvre, F. *J. Chim. Phys.* **1998**, *95*, 1052–1067.
- (4) Mentzen, B. F. *Mater. Res. Bull.* **1992**, *27*, 831–838.

- (5) van Koningsveld, H.; Jansen, H.; van Bekkum, H. *Zeolites* **1990**, *10*, 235–241.
- (6) Mentzen, B. F. *Mater. Res. Bull.* **1995**, *30*, 1333–1340.
- (7) van Koningsveld, H.; Tuinstra, F.; van Bekkum, H.; Jansen, J. C. *Acta Crystallogr.* **1989**, *B45*, 423–431.
- (8) Mortier, W. J. *Compilation of Extra Framework Sites in Zeolites*; Butterworth Scientific Limited: Guildford, 1982; pp 19–31 for FAU and p 53 for MFI.
- (9) Zhenyl, L.; Wangjin, Z.; Qin, Y.; Guanglie, L.; Wangrong, L.; Shunju, W.; Youshi, Z.; Bingxiong, L. *Proceedings of the 7th International Zeolite Conference*; Kodansha Elsevier: Tokyo, Japan, 1986; pp 415–422.
- (10) Lin, J. C.; Chao, K.-J.; Wang, Y. *Zeolites* **1991**, *11*, 376–379.
- (11) Huddersman, K. D.; Rees, L. V. C. *Zeolites* **1991**, *11*, 270–176.
- (12) Mentzen, B. F.; Sacerdote-Peronnet, M.; Bouix, J. C. *R. Acad. Sci., Ser. II* **1992**, *315*, 1073–1078.
- (13) Mentzen, B. F.; Gélin, P. *Mater. Res. Bull.* **1998**, *33*, 109–116.
- (14) Olson, D. H.; Khosrovani, N.; Peters, A. W.; Toby, B. H. *J. Phys. Chem. B* **2000**, *104*, 4844–4848.
- (15) Grey, C. P.; Poshni, F. I.; Gualtieri, A. F.; Norby, P.; Hanson, J. C.; Corbin, D. R. *J. Am. Chem. Soc.* **1997**, *119*, 1981–1989.
- (16) Norby, P.; Poshni, F. I.; Gualtieri, A. F.; Hanson, J. C.; Grey, C. P. *J. Phys. Chem. B* **1998**, *102*, 839–856.
- (17) Breck, D. W. *Zeolite Molecular Sieves, Structure, Chemistry and Use*; John Wiley and Sons: New York, 1974; p 312.
- (18) Lermer, H.; Draeger, M.; Steffen, J.; Unger, K. K. *Zeolites* **1985**, *5*, 131–134.
- (19) Guth, J. L.; Kessler, H.; Wey, R. *Proceedings of the 7th International Zeolite Conference*, Tokyo; Elsevier: Amsterdam, 1986; p 121.
- (20) Tissler, A.; Polanek, P.; Girsch, U.; Müller, U.; Unger, K. K. *Zeolites as Catalysts, Sorbents and Detergent Builders*; Elsevier: Amsterdam, 1989; p 399.
- (21) Bish, D. L.; Post, J. E., Eds. *Modern Powder Diffraction*; Reviews in Mineralogy 20; The Mineralogical Society of America: Washington, DC, 1989; pp 27–31.
- (22) Wiles, D. B.; Young, R. A. *J. Appl. Crystallogr.* **1981**, *14*, 149–151.
- (23) Toby, B. H. EXPGUI, a graphical user interface for GSAS. *J. Appl. Crystallogr.* **2001**, *34*, 210–213.
- (24) Craven, B. M.; Weber, H.-P.; He, X.; Klooster, W. T.; Yang, H. W. The POP system: computer programs to derive electrostatic properties from Bragg reflections. Technical Report, Crystallography Department, University of Pittsburgh, Pittsburgh, PA, 1996.
- (25) Mentzen, B. F.; Bosselet, F. *C. R. Acad. Sci., Ser. II* **1988**, *309*, 539–545.
- (26) Mentzen, B. F.; Lefèbvre, F. *Mater. Res. Bull.* **1995**, *30*, 613–620.
- (27) Mentzen, B. F. *Mater. Res. Bull.* **1995**, *30*, 1193–1200.
- (28) Mentzen, B. F. *C. R. Chim.* **2005**, *8*, 353–368.
- (29) Hunger, M.; Freude, D.; Fenzke, D.; Pfeiffer, H. *Chem. Phys. Lett.* **1992**, *191*, 391–395.
- (30) Mentzen, B. F.; Sacerdote-Peronnet, M. *Mater. Res. Bull.* **1994**, *29*, 1341–1348.
- (31) Mentzen, B. F. *Zeolite News Lett.* **1993**, *10*, 77–90.
- (32) Weber, H. P.; Schulz, H. *J. Chem. Phys.* **1986**, *85*, 475–484.
- (33) Mentzen, B. F.; Lefèbvre, F. *Mater. Res. Bull.* **1997**, *32*, 813–821.
- (34) Mentzen, B. F.; Lefèbvre, F. *Mater. Res. Bull.* **2002**, *37*, 957–970.
- (35) Millet, J.-M.; Mentzen, B. F. *Eur. J. Solid State Inorg. Chem.* **1991**, *28*, 493–504.
- (36) Touboul, M.; Penin, N.; Nowogrockin, G. *J. Solid State Chem.* **1999**, *143*, 260–265.
- (37) Ryu, K. S.; Bae, M. N.; Kim, Y.; Seff, K. *Microporous Mesoporous Mater.* **2004**, *71*, 65–75.
- (38) Schlenker, J. L.; Pluth, J. J.; Smith, J. V. *Mater. Res. Bull.* **1978**, *13*, 901–905.
- (39) *International Tables for X-ray Crystallography*, Vol. III; The Kynoch Press: Birmingham, 1968; p 278.
- (40) Mentzen, B. F.; Bosselet, F. *C. R. Acad. Sci., Ser. II* **1989**, *308*, 1533–1538.
- (41) Fyfe, C. A.; Srobl, H.; Kokotailo, G. T.; Kennedy, G. J.; Barlow, G. E. *J. Am. Chem. Soc.* **1988**, *110*, 3373–3380.
- (42) Mentzen, B. F.; Védrine, J. C. *C. R. Acad. Sci., Ser. II* **1985**, *301*, 1017–1020.
- (43) Yarovoi, S. S.; Yu. Mironov, V.; Solodovnikov, S. F.; Virovets, A. V.; Fedorov, V. E. *Mater. Res. Bull.* **1999**, *34*, 1345–1351.
- (44) Vayssilov, G.; Stauer, M.; Belling, Th.; Neyman, K. N.; Knoezinger, H.; Roesch, N. *J. Phys. Chem. B* **1999**, *103*, 7920–7928.
- (45) Nachtigallova, D.; Nachtigall, P.; Sierka, M.; Sauer, J. *Phys. Chem. Chem. Phys.* **1999**, *1*, 2019–2026.
- (46) K.-P Schröder, Sauer, J.; Leslie, M.; Catlow, C. R. A. *Zeolites* **1992**, *12*, 20–23.

- (47) Derouane, E. G.; Fripiat, J. G. *Zeolites* **1985**, *5*, 165–172.
- (48) Redondo, A.; Hay, P. J. *J. Phys. Chem.* **1993**, *97*, 11754–11761.
- (49) Vetrivel, R.; Catlow, C. R. A.; Colburn, E. A. *Innovation in Zeolite Materials Science*; Elsevier: Amsterdam, 1988; pp 309–315.
- (50) de Vos Burchart, E.; van Bekkum, H.; van de Graaf, B. *Collect. Czech. Chem. Commun.* **1992**, *58*, 681–687.
- (51) Marra, G. L.; Artioli, G.; Fitch, A. N.; Milanesio, M.; Lamberti, C. *Microporous Mesoporous Mater.* **2000**, *40*, 85–94.
- (52) Lamberti, C.; Bordiga, S.; Zecchina, A.; Carati, A.; Fitch, A. N.; Artioli, G.; Petrini, G.; Salvalaggio, M.; Marra, G. L. *J. Catal.* **1999**, *183*, 222–231.
- (53) Njo, S. L.; van Koningsveld, H.; Van de Graaf, B. *J. Phys. Chem.* **1997**, *101*, 10065–10068.
- (54) Jentys, A.; Catlow, C. R. A. *Catal. Lett.* **1993**, *22*, 251–257.
- (55) Oumi, Y.; Matsuba, K.; Kubo, M.; Inui, T.; Miyamoto, A. *Microporous Mater.* **1995**, *4*, 53–57.
- (56) Millini, R.; Perego, G.; Seiti, K. *Zeolites and Related Microporous Materials: State of the Art 1994*; Studies in Surface Science and Catalysis 84; 1994; pp 2123–2129.
- (57) Stave, M. S.; Nicholas, J. B. *J. Phys. Chem.* **1995**, *99*, 15046–15061.
- (58) Alvarado-Swaisgood, A. E.; Barr, M. K.; Hay, P. J.; Redondo, A. *J. Phys. Chem.* **1991**, *95*, 10031–10036.
- (59) Lonsinger, S. R.; Chakraborty, A. K.; Theodorou, D. N.; Bell, A. T. *Catal. Lett.* **1991**, *11*, 209–217.